Current Waveform Optimization for Force Ripple Compensation of Linear Synchronous Motors

Christof Röhrig
Department of Electrical Engineering
University of Hagen
D-58084 Hagen, Germany
Email: christof.roehrig@fernuni-hagen.de

Abstract—**Linear synchronous motors are finding expanded use in high-performance applications where high speed and high accuracy is essential. The main problem in improving the tracking performance of linear synchronous motors is the presence of force ripple caused by mismatched current waveforms and unbalanced motor phases or amplifier gains. This paper presents a method to optimize the waveform of the phase currents in order to generate smooth force. The optimized current waveforms produces minimal copper losses and maximizes motor efficiency. The waveforms are implemented in a waveform generator of the motion controller and approximated with Fourier series. The optimization method proposed here consist of three stages. In every stage different harmonic waves of the force ripple are reduced. A comparison of the tracking performance with optimized waveforms and with sinusoidal waveforms shows the effectiveness of the method.**

I. Introduction

Permanent magnet (PM) linear synchronous motors (LSM) are beginning to find widespread industrial applications, particularly for tasks requiring a high precision in positioning such as various semiconductor fabrication and inspection processes [1]. The main benefits of PM LSMs are the high force density achievable and the high positioning precision and accuracy associated with the mechanical simplicity of such systems. The electromagnetic force is applied directly to the payload without any mechanical transmission such as chains or screw couplings. This greatly reduces nonlinearities and disturbances caused by backlash and additional frictional forces [2]. Todayt's state-of-the-art linear motors can, typically, achieve velocities up to $10\,m/s$ and accelerations of $10\,g$ [3].

The more predominant nonlinear effects underlying a PM LSM system are friction and force ripple arising from imperfections in the underlying components. In order to avoid force ripple different methods have been developed. In [4] several techniques of torque ripple minimization for rotating motors are reviewed. In [5] a force ripple model is developed and identification is carried out with a force sensor and a frictionless air bearing support of the motor carriage. Position-triggered repetitive control is proposed in [6] in order to reduce the effect of force ripple. Other approaches are based on iterative learning control [7] or adaptive control [8]. The main problem in adaptive control is the low signal-to-noise ratio at high motor speeds [9]. In [10] a force ripple compensation method for PM LSM systems

with electronic commutated servo amplifiers was presented. The parameters of the force ripple model are identified in an offline procedure.

In this paper a force ripple compensation method for software commutated servo amplifiers is proposed. The additional input signal of a software commutated amplifier is used to optimize the operation of the motor. The paper proposes a method for the design of the input signals of the amplifier for minimization of force ripple an maximization of motor efficiency. The waveforms of the phase currents are optimized in order to get smooth force and minimal copper losses. In order to optimize the currents waveforms the force functions of the phases are identified. The identification is performed by measuring the control signals in a closed position control loop. The waveform generation is directly integrated in the software commutation module of the motion controller. The optimal current waveforms are approximated with Fourier series.

II. Experimental Setup

A. Linear Motor

The motors considered here are PM LSM with epoxy cores. A PM LSM consists of a secondary and a moving primary. There are two basic classifications of PM LSMs: epoxy core (i.e. non-ferrous, slotless) and iron core. Epoxy core motors have coils wound within epoxy support. These motors have a closed magnetic path through the gap since two magnetic plates "sandwich" the coil assembly [11]. The secondary induces a multipole magnetic field in the air gap between the magnetic plates. The electromagnetic thrust force is produced by the interaction between the permanent magnetic field in the secondary and the magnetic field in the primary driven by the phase currents of the servo amplifier. The linear motor under evaluation is a current-controlled three-phase motor driving a carriage supported by roller bearings. The motor drives a mass of total $2\,Kg$ and is vertical mounted.

B. Servo Amplifier

The servo amplifier employed in the setup is a PWM type with closed current control loops. The software commutation of the three phases is performed in the motion controller with the help of the position encoder. This commutation method requires two current command signals, from the controller.

The third phase current depends on the others, because of the wye motor connection:

$$i_C = -i_A - i_B \tag{1}$$

The maximum input signals u_A, u_B of the servo amplifier ($\pm 10V$) correlate to the peak currents of the current loops. The dynamics of the servo amplifier will not be considered as they play a minor role in the dynamics of the whole system.

III. System Modeling

The thrust force is produced by the interaction between the magnetic field in the secondary and the magnetic field of the phase windings. The thrust force is proportional to the magnetic field and the phase currents i_A, i_B, i_C. The back-EMF induced in a phase winding (e_A, e_B, e_C) is proportional to the magnetic field and the speed of the motor. The total thrust force F_{thrust} is the sum of the forces produced by all phases:

$$\dot{x} \, F_{thrust} = \sum_p e_p(x) \, i_p \; ; \qquad p \in \{A, B, C\} \tag{2}$$

The back-EMF waveform $\frac{e_p}{\dot{x}}$ can also be interpreted as the force function of the phases p ($K_{M_p}(x)$).

$$F_{thrust} = \sum_p K_{M_p}(x) \, i_p \; ; \qquad p \in \{A, B, C\} \tag{3}$$

Force ripple is an electro-magnetic effect and causes a periodic variation of the force constant. Only if the back-EMF waveforms are sinusoidal and balanced, symmetric sinusoidal commutation of the phase currents produces smooth force. Force ripple occurs if the motor current is different from zero, and its absolute value depends on the required thrust force and the relative position of the primary to the secondary.

There are several sources of force ripple:

- motor
  - harmonics of back-EMFs
  - amplitude imbalance of back-EMFs
  - phase imbalance of back-EMFs
- amplifier
  - offset currents
  - imbalance of current gains

Offset currents lead to force ripple with the same period as the commutation period. This force ripple is independent of the desired thrust force. Amplitude or phase imbalance of the motor and imbalance of amplifier gains lead to force ripple with half commutation period which scale in direct proportion to the desired thrust force. A kth order harmonic of a back-EMF produces $(k-1)^{th}$ and $(k+1)^{th}$ order harmonic force ripple if a sinusoidal current is applied.

Force ripple with the same period as the commutation period is independent of the desired thrust, all higher order harmonics scale in direct proportion to the desired thrust because of the linearity of the force equation (2). Fig. 1 shows the block diagram of a servo system with PM LSM. The friction force is modeled with a kinetic friction model. In the kinetic friction model the friction force is a function of velocity only.

IV. Compensation of Force Ripple

The method for force ripple compensation consist of three stages. In every stage different harmonic waves of the ripple spectrum are reduced. In order to optimize the waveforms of the currents, identification of the force functions $K_{M_p}(x)$ is essential. The main idea of the proposed method is to identify the force functions in a closed position control loop by measuring the control signal u of the position controller at constant load force F_{load} as a function of the position x. Neither additional sensor nor device for position adjustment are necessary. In the experimental setup the constant load force is produced by the force of gravitation. In order to avoid inaccuracy by stiction the measurement is achieved with moving carriage.

A. Experimental Analysis of Force Ripple

In order to analyze the force ripple of the motor a sinusoidal reference current is applied:

$$u_A(u, \vartheta) = u \frac{2}{3} \sin(\vartheta(x)) + o_A \tag{4}$$

$$u_B(u, \vartheta) = u \frac{2}{3} \sin\left(\vartheta(x) + \frac{2\pi}{3}\right) + o_B$$

$$\text{with} \quad \vartheta(x) = \frac{\pi}{\tau_p}(x - x_0)$$

where u_A, u_B are the current commands of the two phases, u is the output of the position controller, x is the position of the carriage, τ_p is the pole pitch and x_0 is the zero position with maximum force. In the first stage, the DC components of the command signals (o_A, o_B) are chosen equal zero. Fig. 2 shows the control signals u, u_A, u_B versus the position x. The ripple on the command signal u is caused by force ripple. The controller compensates the force ripple by changing the control signal over the position. If the speed of the motor is high, the force ripple increases the tracking error.

Frequency domain analyses of the control signal indicates that the fundamental corresponds to the commutation period $2\tau_p$. In order to estimate the parameters of the ripple a least square estimation of the model parameters (5) was applied. A least square estimation is chosen, because noise overlays the control signal.

$$f(x, \boldsymbol{\theta}) = \theta_1 + \theta_2 \, x + \sum_{k=1}^{N} \left(\theta_{2k+1} \sin\left(k\,\pi \frac{x}{\tau_p}\right) \right. \tag{5}$$
$$\left. + \theta_{2k+2} \cos\left(k\,\pi \frac{x}{\tau_p}\right) \right)$$
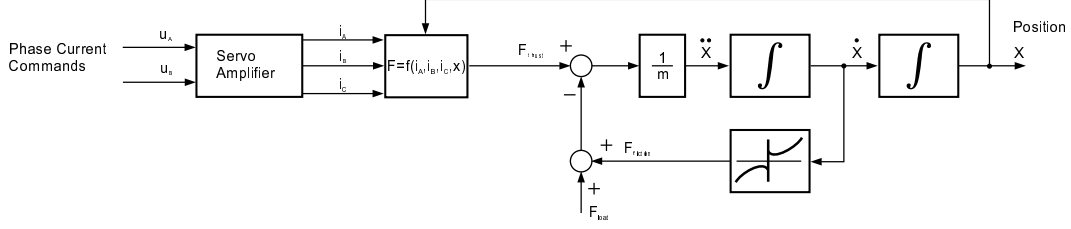
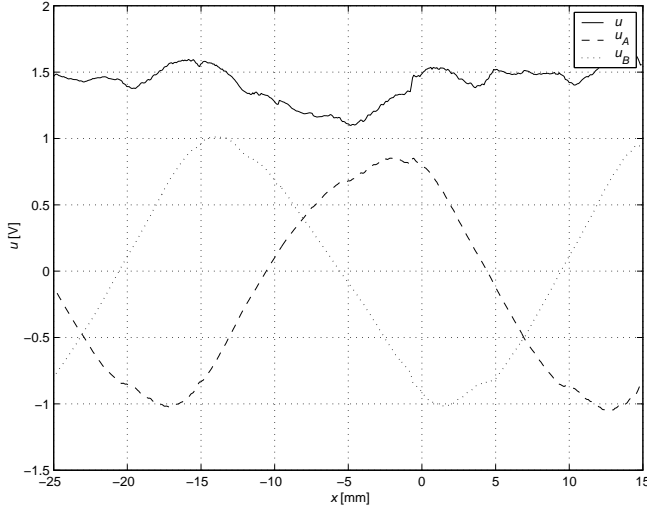Fig. 1. Nonlinear model of a PM LSM servo system

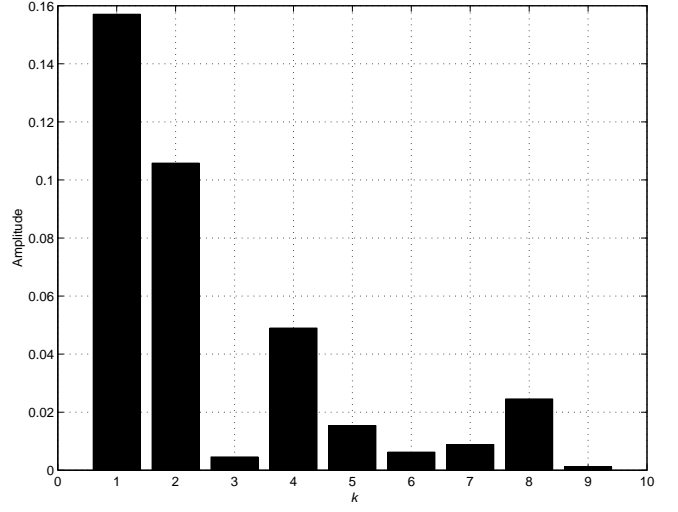Fig. 2. Phase currents at load force $F_{load} = 20N$

Fig. 3. Spectrum of the command signal

where θ_k are the estimated parameters. With θ_1 the sum of load force and friction is estimated. The modeled spring force (θ_2) is necessary, because the control signal rises with rising positions. This is caused by wire chains. Fig. 3 shows the amplitudes of the sinusoids $\sqrt{\theta_{2k+1}^2 + \theta_{2k+2}^2}$ versus the order of the harmonics k.

The fundamental period ($k = 1$) corresponds to $2\,\tau_p$ ($30mm$). The amplitude of this sinusoid is independent of the load force. The higher order harmonics ($k > 1$) scale in direct proportion to the load force because of the linearity of the force equation (3).

B. Compensation of Current Independent Force Ripple

The curve of the phase current command u_A in Fig. 2 shows that this current independent ripple produces a DC component of the current command. This DC component compensates offsets in the analog circuits of the servo amplifier. In the first stage the DC components of the phase current commands are calculated and applied in (4).

$$o_A = \frac{a}{3} \cos \alpha \qquad (6)$$

$$o_B = \frac{a}{2\sqrt{3}} \sin \alpha - \frac{a}{6} \cos \alpha$$

where a is the amplitude and α is the phase of the fundamental of the ripple. In an servo system with iron-less motor the DC components compensate the offsets of the amplifier. If an iron motor is employed, the DC components generate a sinusoidal force which compensates the cogging force.

C. Identification of Force Functions

In the next stage the force functions of the phases are identified. In order to optimize the current waveforms, it is essential to identify the amplitudes and phases of the force functions properly. The motor efficiency depends directly on a properly identified commutation zero position x_0 which depends on the phase lag of the force functions. In [12] a sinusoidal commutation is applied to identify the force functions. With the help of sinusoidal commutation it is impossible to identify the force functions independently. In
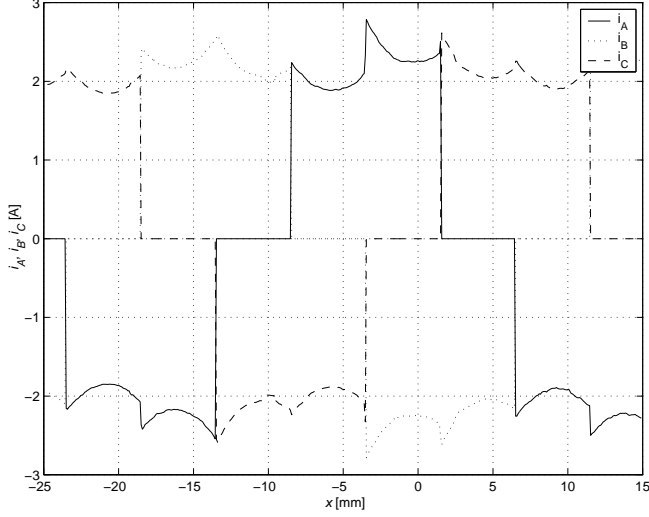
Fig. 4.   Square-wave commutation

Fig. 5.   Optimized waveforms

this paper a square-wave commutation is applied, in order to identify the force functions independently.

Fig. 4 shows the phase currents i_A, i_B, i_C over the position x, when square-wave commutation is applied. The minimum values of the phase currents correlate to the maximum values of the force functions. In square-wave commutation always two phases share the same absolute value of current, which depends on the control signal u and the current gains of the amplifier K_{S_p}.

$$|i_p| = K_{S_p} \frac{u}{\sqrt{3}} ; \qquad p \in \{A,B,C\} \qquad (7)$$

Since only two phase currents are independent, the force equation can be described as:

$$F_{thrust} = K_A(\vartheta) u_A + K_B(\vartheta) u_B \qquad (8)$$

Since the load force is constant over the position, it is possible to identify the force functions K_A and K_B with the measured phase current control signals (u_A, u_B).

D. Current Waveform Optimization

Aim of the current waveform optimization is to obtain reference waveforms of the phase currents which generates smooth force. The main condition of the optimization is $F_{thrust} = const$ in (8). The optimal current waveforms for generation of smooth force are not uniquely defined unless additional constraints are defined. The constraint considered here are:

- The sum of all phase currents is equal zero (1).
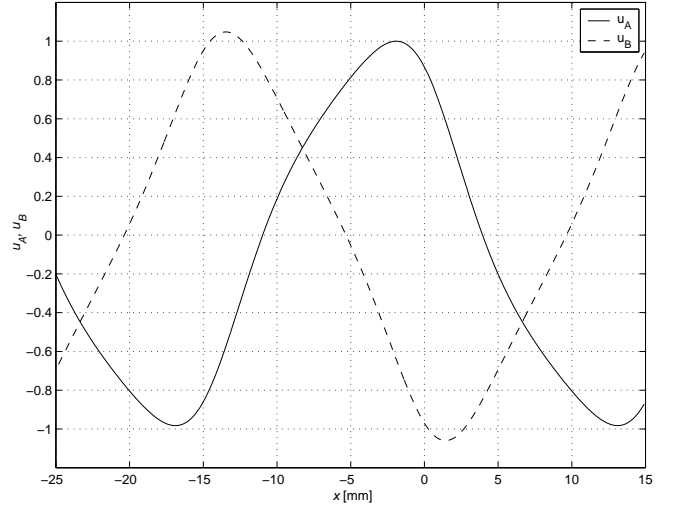- Minimum copper losses (9, 10)

$$P_{cu}(x) = \sum_p R_p i_p^2(x) ; \qquad p \in \{A,B,C\} \qquad (9)$$

$$\Rightarrow \min_{u_A, u_B} f(u_A, u_B) = u_A^2 + u_B^2 + u_A u_B \qquad (10)$$

In Fig. 5 the optimized phase current waveforms are shown. In order to implement the waveforms in the motion controller, the following approximation is applied:

$$u_A(u, \vartheta) = u \frac{2}{3} \left(\sin(\vartheta) + a_3 \sin(3\vartheta + \alpha_3) \right) + o_A \qquad (11)$$

$$u_B(u, \vartheta) = u \frac{2}{3} \left(\sin\left(\vartheta + \frac{2\pi}{3}\right) + b_3 \sin(3\vartheta + \beta_3) \right) + o_B$$

Fig. 6 compares the commutation functions. The dashed line shows the control signal when a sinusoidal commutation plus offset compensation is employed (4). The solid line shows the control signal when optimized waveforms are applied (11). The ripple of the control signal is significantly reduced when the optimized waveforms are applied.

E. Fine tuning of the waveforms

After the numerical optimization the motor efficiency is maximized, but the control signal still consists of some higher order ripple. The higher order ripple is caused by unmodeled harmonics of the force functions. In order to reduce some of the higher order ripple a fine tuning of the waveforms is performed. The main idea of the fine tuning algorithm is to measure the phase current control signals at constant load force. The fine tuning is performed with previously optimized waveforms in order to maximize motor efficiency. The still remaining higher order ripple of the control signal modulates
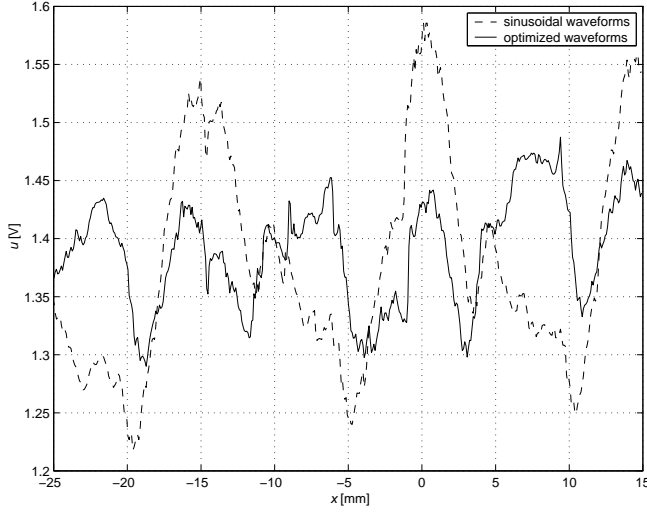
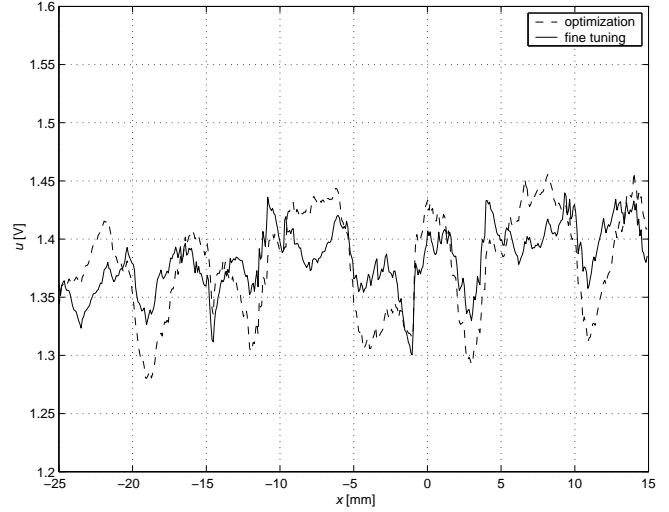Fig. 6. Command signals with sinusoidal versus optimized waveforms

Fig. 8. Command signals with optimized versus fine tuned waveforms

the optimized waveforms. The fine tuning algorithm approximates the shapes of the measured phase command signals with Fourier series. Fig. 7 compares the measured phase command signals with the approximation. The approximation adds one additional harmonic to the approximation in (11). Fig. 8 compares the commutation functions of the second stage with the third stage.
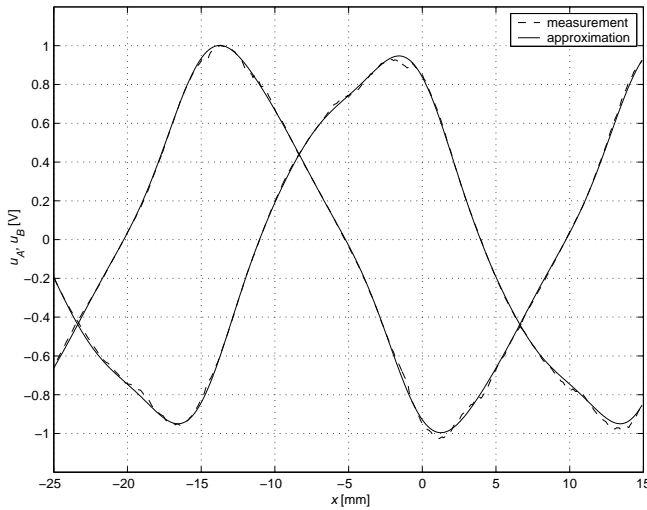

Fig. 7. Fine Tuned Waveforms

Fig. 9 compares the command signal spectrum of the optimization process. The upper left graph shows the spectrum before any optimization is applied. The upper right graph shows the spectrum after the offset compensation is applied. The fundamental is significantly reduced. In the lower left graph the spectrum of the control signal of numerically optimized waveforms is shown. This stage reduces the 2th

order harmonics. The lower right graph shows the spectrum of the control signal for fine tuned waveforms. This last stage reduces the 2th and 4th order harmonics. After the fine tuning of the waveforms no dominant harmonic exists in the control signal.
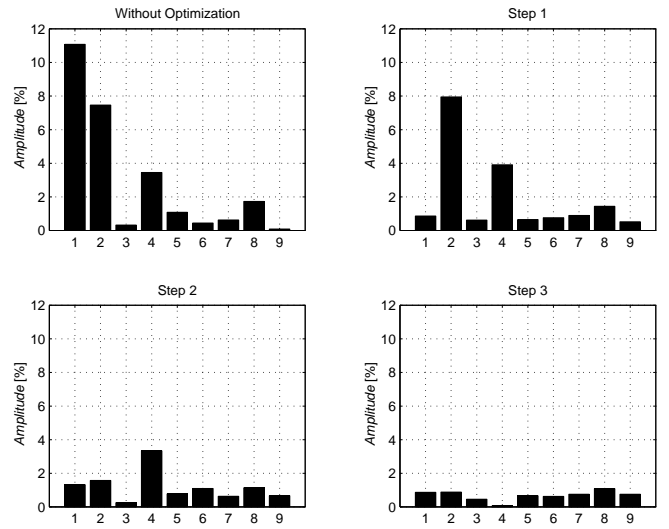

Fig. 9. Spectrum of the command signal

F. Controller Design

Fig. 10 shows the block diagram of the servo control system. In order to achieve a better tracking performance, a feedforward controller is applied. Feedback control without feedforward control always introduces a phase lag in the command response. Feedforward control sends an additional output, besides the feedback output, to drive the servo amplifier input to desired thrust force. The feedforward control
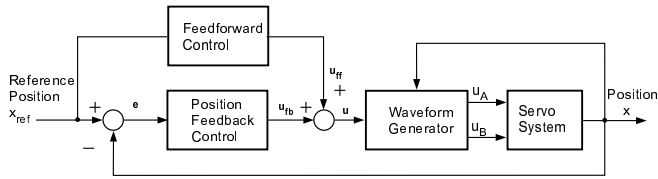
Fig. 10.   Controller design

compensates the effect of the carriage mass and the friction force. The friction force is modeled by a kinetic friction model and identified with experiments at different velocities. The stability of the system is determined by the feedback loop (PD controller). The compensation of the force ripple is completely performed in the waveform generator with Fourier series approximation. Fig. 11 compares the tracking error of a movement without ripple compensation with the movement with ripple compensation. In this measurement, the carriage moves from position $-25mm$ to position $15mm$ and back to position $-25mm$ with $v_{max} = 200mm/s$. If the ripple compensation is applied, the tracking error is reduced significantly.
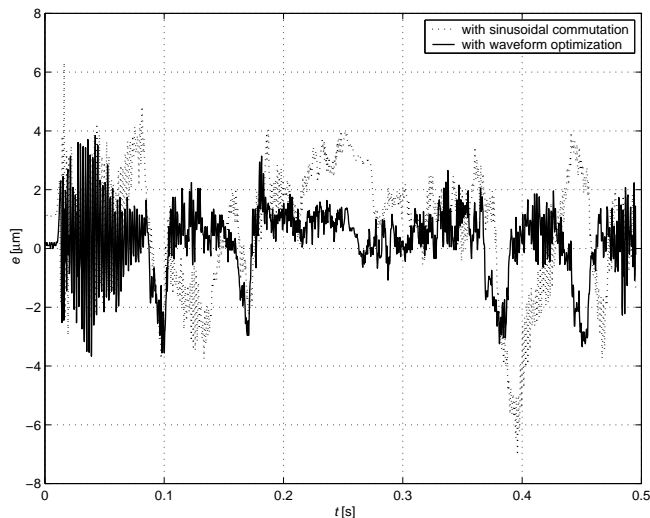

Fig. 11.   Tracking error

V. CONCLUSION

In this paper, a method for optimization of the current waveforms is presented. The optimized current waveforms generate smooth force and produce minimal copper losses which maximizes motor efficiency. The optimized current shapes are valid for any velocity and any desired thrust force. In order to identify the force functions, no additional sensors are required. Experiments show that the tracking performance is significantly improved if the optimized waveforms are applied. The described optimization method is implemented successfully in the motion controllers of several machines for semiconductor production to improve the tracking performance.

VI. REFERENCES

[1] A. Basak, *Permanent-Magnet DC Linear Motors*. Oxford: Clarendon Press, 1996.

[2] G. Pritschow, "A Comparison of Linear and Conventional Electromechanical Drives," *Annals of the CIRP*, vol. 47, no. 2, pp. 541–548, 1998.

[3] D. Howe, R. Clark, and Z. Zhu, "Status of Linear Drive Technologies in Europe," in *Proceedings of the Third International Symposium on Linear Drives for Industry Applications*, Oct. 2001, pp. 468–473.

[4] T. M. Jahns and W. L. Soong, "Pulsating Torque Minimization Techniques for Permanent Magnet AC Motor Drives - A Review," *IEEE Transactions on Industrial Electronics*, vol. 43, no. 2, pp. 321–330, 1996.

[5] P. Van den Braembussche, J. Swevers, H. Van Brussel, and P. Vanherck, "Accurate Tracking Control of Linear Synchronous Motor Machine Tool Axes," *Mechatronics*, vol. 6, no. 5, pp. 507–521, 1996.

[6] P. Van den Braembussche, J. Swevers, and H. Van Brussel, "Linear Motor Ripple Compensation Using Position-triggered Repetitive Control," in *Proceedings of the IFAC Workshop on Motion Control*, Grenoble, France, 1998, pp. 353–357.

[7] T. Lee, K. Tan, S. Lim, and H. Dou, "Iterative Learning of Permanent Magnet Linear Motor with Relay Automatic Tuning," *Mechatronic*, vol. 10, no. 1-2, pp. 169–190, 2000.

[8] L. Xu and B. Yao, "Adaptive Robust Precision Motion Control of Linear Motors with Ripple Force Compensation: Theory and Experiments," in *Proceedings of the IEEE Conference on Control Applications*, Sept. 2000, pp. 373–378.

[9] A. Seguritan and M. Rotunno, "Adaptive Torque Pulsation Compensation for a High-torque DC Brushless Permanent Magnet Motor," in *Proceedings of the 15th IFAC World Congress on Automatic Control*, Barcelona, Spanien, July 2002.

[10] C. Röhrig and A. Jochheim, "Identification and Compensation of Force Ripple in Linear Permanent Magnet Motors," in *Proceedings of the American Control Conference 2001*, June 2001, pp. 2161–2166.

[11] *LE Series Linear Motor Systems, Motor Integration Manual LEA, LEB, LEC & LEM Linear Motors*, Anorad Corporation, Sept. 1999.

[12] C. Röhrig and A. Jochheim, "Motion Control of Linear Synchronous Motors with Force Ripple Compensation using Current Shaping," in *Proceedings of the 15th IFAC World Congress on Automatic Control*, Barcelona, Spain, July 2002.